1-1-2008

Visualization of Convection Patterns Near an Evaporating Meniscus using micro-PIV

Pramod Chamarthy

Hemanth Dhavaleswarapu

S V. Garimella
Purdue University, sureshg@purdue.edu

Jayathi Y. Murthy
School of Mechanical Engineering, Purdue University, jmurthy@purdue.edu

Steven Wereley
Purdue University - Main Campus, wereley@purdue.edu

Visualization of Convection Patterns near an Evaporating Meniscus using µPIV

Pramod Chamarthy, Hemanth K. Dhavaleswarapu, Suresh V. Garimella*, Jayathi Y. Murthy and Steven T. Wereley

Cooling Technologies Research Center, School of Mechanical Engineering
Purdue University, West Lafayette, IN 47907, USA

Summary. Experimental visualizations of the 3D convection patterns generated near an evaporating meniscus in horizontally oriented capillary tubes are presented. These patterns are caused due to the differential evaporation along the meniscus. In this study, transparent capillary tubes with refractive index close to that of the evaporating liquid were used to minimize refraction effects and obtain velocity vectors near the walls. Polystyrene fluorescent particles of 0.5 µm diameter suspended in methanol were used to make the measurements in tubes of 75, 200 and 400 µm diameter. For the 75 µm tube, gravity was observed to have no effect on the flow patterns and an axisymmetric counter-rotating vortex pair was present along the horizontal and vertical center planes, suggesting the presence of a toroidal vortex near the meniscus. With an increase in tube size, buoyancy effects became apparent as the axisymmetric pattern broke down. A counter-rotating symmetric vortex pair was observed in the horizontal center plane, whereas in the vertical center plane, a single vortex dominated the flow and pushed the secondary vortex to a corner. Particle streak and µPIV images were obtained in multiple horizontal planes and a vertical center plane to understand this 3D flow behavior.

Keywords. *Flow Visualization, Thermocapillary convection, Marangoni convection.*

____

*Corresponding author. E-mail: **sureshg@purdue.edu**

1 Introduction

Surface tension plays an important role in a variety of problems in hydrodynamics and heat and mass transfer [1] which involve interactions between two immiscible fluids. In the presence of surface tension gradients, shear stresses arise along the interface resulting in fluid motion which propagates into the bulk of the liquid through viscous coupling. A surface tension gradient-driven phenomenon, generally known as the Marangoni effect [2], can be caused by gradients present in concentration, electric field or temperature. The flows generated due to a temperature gradient present along the interface are called thermocapillary flows.

In general, thermocapillary and buoyancy effects are present simultaneously. Typically, buoyancy-driven motion dominates at liquid thicknesses greater than 1 mm, while thermocapillary motion dominates when the liquid thickness is less than 1 mm and/or in microgravity environments [3]. It is the combination of these two forces that gives rise to instability in the flow patterns. In thermocapillary convection instability, temperature gradients exist primarily parallel to the interface, in which case even a small temperature gradient will initiate a flow [1]. In such cases, the basic flow pattern at very low temperature gradients is considered to be either a steady one-dimensional or two-dimensional pattern, which at higher temperature gradients becomes a steady or unsteady three-dimensional flow pattern. Davis [4] provided a detailed discussion of the various instabilities observed in thermocapillary flows.

Several numerical studies [5-12] have investigated thermocapillary convection and/or combined thermocapillary and buoyancy-driven convection in rectangular containers, and have shown that the thermocapillary convection substantially augments heat transfer by a factor 2 to 2.5 in comparison to a model without convection. Lee et

2

al. [13] studied the combined buoyant-thermocapillary convection in rectangular containers through experiments and numerical analysis. They found that for imposed temperature differences greater than a critical value, the flow becomes oscillatory with periodic variation of the temperature field. These oscillations disturb the two-dimensional velocity and temperature fields, forcing them to become three-dimensional and periodic in time.

A number of experimental approaches have also been employed for measuring thermocapillary convection. Wozniak et al. [14-16] applied particle image velocimetry (PIV) and laser-speckle velocimetry to measure the thermocapillary convection and buoyancy effects around a bubble. Kamotani and Ostrach [17] used PIV to measure the unicellular flow pattern in silicone oil contained in a heated circular container. Braunsfurth and Homsy [18] employed particle tracking velocimetry (PTV) and observed the primary transition from 2D flow to steady 3D rolls and further to an unsteady 3D pattern with increased temperature gradient between the side walls in a square cavity. Recently, Ward and Duan [19] studied thermocapillary convection in water by measuring the deflection of a cantilever probe inserted into the flow. This method cannot be used to obtain the entire flow map because of the intrusive nature of the probe and its dimensional constraints.

In many engineering applications involving two-phase heat transfer, both thermocapillary and buoyancy forces play important roles. The stability of an evaporating meniscus inside a capillary structure was studied by Pratt and Hallinan [20] to better understand the working of heat pipes and capillary pumped loop devices. Kim and Wayner [21], Hohman and Stephan [22] and Swanson and Herdt [23] studied the stability of an evaporating meniscus in a capillary tube. Pratt et al. [24] investigated the

effect of a temperature gradient on an evaporating meniscus and observed that the thermocapillary stresses generated along the meniscus cause it to recede. None of these studies investigated the flow inside the liquid and the change in hydrodynamics under the presence of temperature gradients. Molenkamp [25] studied the evaporation from micro grooves and observed that thermocapillary convection enhanced the overall heat and mass transfer.

More recently, Buffone et al. [26, 27, 3, 28] made flow measurements using μPIV to investigate thermocapillary convection and instabilities near an evaporating meniscus in glass capillaries of diameters ranging from 600 μm to 1630 μm. However, their experimental setup introduced optical distortions because of the curvature of the glass tube making it difficult to obtain measurements near the wall; only the central 70% of the tube cross-section could be observed. They studied the flow pattern along horizontal and vertical center planes and observed periodic instabilities in the meniscus pinned at the tube end. Because of limitations in their experimental approach and the unsteady nature of the flow, a physically realizable flow profile could not be obtained.

The present work quantitatively investigates the 3D convection pattern near an evaporating meniscus at sub-millimeter length scales. Larger length scales introduce higher temperature gradients, and as a result, can induce instabilities. Hence, the simplest case of a steady thermocapillary convection pattern generated by an evaporating meniscus in microtubes of diameter 75, 200 and 400 μm is studied, under room temperature conditions. Detailed μPIV measurements were made at multiple measurement planes to understand the three-dimensional flow behavior. Two different test setups were employed to enable visualization in orthogonal planes. A complete 3D

flow profile of steady thermocapillary convection in a capillary tube has not been reported before.

2 Experimental Setup and Procedures

A standard epi-fluorescent micro particle image velocimetry (μPIV) [29] setup is used to make highly resolved spatial measurements of the flow field near the evaporating meniscus. The experimental apparatus for obtaining measurements at different horizontal planes is shown in Fig. 1, and consisted of an inverted Nikon microscope (TE 200), a two-cavity frequency-doubled ND-YAG laser (New Wave Research, Inc.) and an interline transfer Charge Coupled Device (CCD) camera (LaVision Inc., Imager Intense), all of which are set up on an optical table to minimize mechanical vibrations. The wavelength and pulse width of the laser beam are 532 nm and 3–5 ns, respectively. A beam expander assembly is installed between the laser and the microscope to match the diameter of the laser beam to that of a white light source. The beam expander is configured with a negative and a positive lens in a Galilean telescope arrangement; a 5 deg diffuser situated between the two lenses expands the original 3 mm diameter laser beam to 5 cm to prevent damage to the internal optics of the microscope. After passing through the beam expander assembly, the laser beam enters the microscope. The path followed by the illuminating beam through the microscope, dichroic filter cube and the objective lens is illustrated in Fig. 1. The filter cube consists of an exciter (green filter), an emitter (red filter), and a dichroic mirror. After passing through the exciter, the incoming laser beam reaches the dichroic mirror, which is designed to reflect short wavelengths (λ_{abs} ~542 nm) and transmit long-wavelength light. The laser beam (λ_{abs} ~ 542 nm) is therefore directed towards the specimen through the objective lens. The longer wavelength light emitted by the fluorescent specimen is transmitted through the

5

dichroic mirror towards the emitter which blocks any short wavelengths present and sends the signal to the camera. The images are captured by the CCD camera with a time difference of 20 ms between successive images. The images are later analyzed using the custom-written PIV software, EDPIV[30].

< Figure 1 >

The test piece as shown in Fig. 1 consists of a Fluorinated Ethylene Propylene (FEP) capillary tube filled with methanol. The FEP tube is surrounded by a water jacket enclosed between two glass slides and placed such that the tube axis is orthogonal to the direction of gravity. The comparable refractive indices of FEP, methanol and water aid in minimizing optical distortions so that accurate velocity measurements may be obtained near the tube walls. Figure 2(a) shows an image obtained in a FEP tube without the water jacket and the distortions introduced due to the curvature of the tube can be seen clearly; Fig. 2(b) shows a refractive-index-matched image obtained in a FEP tube with the water jacket present in which there are minimal distortions.

< Figure 2 >

Tubes of length 70 mm are filled to two-thirds of their length with methanol such that both the free surfaces are at least 10 mm away from the tube ends. Due to the micro-irregularities present on the tube surface, one of the menisci is pinned while the other recedes to compensate for the evaporation occurring at both the ends. Images for the current work are obtained at the stationary meniscus. The situation where the meniscus is pinned at the end of the tube is not considered for the visualizations due to the optical distortions that resulted. The evaporation rates in the 400, 200 and 75 μm diameter tubes are found to be 0.96, 0.28 and 0.008 ng/s, respectively. The contact angle of methanol in FEP capillary tubes is determined to be 50±3 degrees from the

experimental images.   The contact angle and the evaporation rates were fairly

independent of the meniscus location inside the tube. The water bath surrounding the

tube approximates an isothermal boundary condition at the walls. All experiments are

conducted at room temperature and under atmospheric pressure conditions.   No

instability is observed at the stationary meniscus located inside the tube in contrast to

the unsteady flow pattern reported by Buffone et al. [3] for a meniscus pinned at the end

of the tube. The lack of instability may be due to the lower evaporation rates and low

temperature gradients in the present work. Capillary tubes with internal diameters of

75, 200 and 400 μm are used to explore tube-size effects on convection.

Fluorescent polymer micro spheres (Duke Scientific Co.) with a density of 1.05

g/cm^3 and diameter of 0.5 μm are used to seed the fluid. These particles absorb green

light (λ ~ 542 nm) and emit red light (λ ~ 612 nm). Their settling velocity is estimated

to be 4.2 x 10^{-8} m s^{-1} which is 4 orders of magnitude smaller than the mean fluid

velocity of 10^{-4} m s^{-1}. Hence, the sedimentation time of the particles for the smallest

tube investigated (~ 75 μm) is estimated to be of the order of several hours, which is

large in comparison to the typical imaging duration (~ 180 s). The presence of particle

clumps near the meniscus is observed to change the flow pattern.   Hence, a low

particulate concentration (volume fraction ~ 1:200,000) is used to avoid such clumps.

< Figure 3 >

Buoyancy effects were investigated by visualizing the flow along the vertical

center plane.   These experiments are conducted using an upright Nikon Eclipse

(ME600) microscope with an interline transfer CCD camera (Roper Scientific

Photometrics, CoolSNAP HQ). As the microscope objective lens (Nikon CFI60) is

infinity-corrected, a 45 deg mirror is placed between the lens and the camera as shown

in Fig. 3 to image the vertical center plane. Metamorph software was used to obtain the images. A Nikon mercury arc lamp was used as the illumination source, with an exposure time of 30 ms for obtaining the streak images.

3 Results and Discussion

To identify the convection patterns, µPIV measurements are made along seven different horizontal planes, and the vertical center plane, as illustrated in Fig. 4 near the evaporating meniscus in a 400 µm capillary tube. For the study of buoyancy effects, flow visualization was conducted along the vertical center planes of the 75 and 200 µm capillary tubes as well.

< Figure 4 >

3.1 3D flow pattern

As the flow did not exhibit any unsteady behavior, a large number of image pairs are used to obtain averaged velocity vectors. Figure 5(a) shows the raw image obtained by the superposition of 100 image pairs. The meniscus shape, the uniform distribution of particles and the lack of particle clumps are all clearly observed in this image. In order to determine the number of images needed to obtain accurate measurements, the images are analyzed individually and averaged over increasing numbers of images. For a small number of image pairs, the averaged error is large, and then decreases progressively as the number of image pairs is increased as illustrated in Fig. 5(b). It can be seen that the error reaches a minimum ($\sim$ 0.5%) for image pairs over 100 in number.

The thickness of the measurement plane is estimated based on the relationship for the depth of correlation developed by Meinhart et al.[31]. For a 20X, 0.5 N.A.

8

objective with 0.5 μm particles suspended in water, the thickness of the measurement plane is calculated to be 7 μm.

< Figure 5 >

Figure 6(a-g) shows the μPIV measurements obtained at the seven horizontal planes marked in Fig. 4 for a 400 μm tube. Only a subset of the planar velocity vectors $\mathbf{V}$ obtained is shown to improve clarity. The magnitude of vorticity ω calculated using $\omega = \nabla \times \mathbf{V}$ with the origin fixed at the left bottom corner of the image is shown in the contours. The vorticity magnitude was evaluated by central differencing at the interior points and by backward differencing at the boundaries (tube walls and meniscus surface) to evaluate the vorticity magnitude. The shape of the meniscus was extracted from superimposed images as in Fig. 5(a) using a MATLAB program. Streamtraces are also plotted to clearly illustrate the flow pattern; the tube walls and the meniscus surface are also delineated. The flow profile along the horizontal center plane Fig. 6(d) exhibits two symmetric, counter-rotating vortices. This is attributed to the differential evaporation taking place along the meniscus which makes the liquid near the walls cooler than the liquid at the meniscus center. Since surface tension decreases with an increase in temperature for methanol (and for most liquids), a surface tension gradient drives the liquid at the center of the meniscus towards the wall along the interface, setting up the observed symmetrical vortex pattern due to viscous coupling.

< Figure 6 >

The velocity profiles measured at the other six horizontal planes – three top planes and three bottom planes – show the asymmetric nature of the flow along the vertical direction. Though the top plane 1 and bottom plane 1 are equidistant from the center plane, the velocity profiles at these planes are completely different indicating a

3D flow pattern. In the top plane 1, vortices are found to lose their strength and are pushed towards the wall with the axial flow directed towards the meniscus. In the bottom plane 1, on the other hand, the flow is directed almost uniformly away from the meniscus. This difference becomes more apparent in the top plane 2 where two small vortices are present at the corners of the meniscus with the bulk flow being towards the meniscus; in the top plane 3, the vortices are altogether absent. In the bottom planes 2 and 3, the flow is uniformly directed away from the meniscus. This analysis of flow in the different horizontal planes indicates a symmetric counter-rotating vortex pair that grows from the top plane 2 to the center plane and vanishes beyond this region. The flow towards the meniscus in the top planes and away from the meniscus in the bottom planes indicates the presence of flow asymmetry along the vertical center plane. The velocity magnitudes along the center line of the seven planes at a distance 80 μm away from the liquid-vapor interface are listed in Table 1.

< Figure 7 >

Flow visualization along the vertical center plane of the meniscus for this flow is shown in Fig. 7. The direction of gravity is shown by the closed arrow. A single large counter-clockwise vortex is seen to occupy much of the plane, with a smaller vortex present near the top wall. By considering the measurements along the horizontal planes and the vertical center plane together, a picture of the complete 3D velocity field emerges, revealing an asymmetric toroidal vortex present near the meniscus.

The observed asymmetry in the flow pattern is caused by buoyancy effects, since the tube axis is oriented orthogonal to the direction of gravity. As evaporation occurs at the interface, it renders the meniscus region relatively cooler than the bulk liquid away from the meniscus. This difference in temperature drives buoyancy-driven convection

along the vertical center plane. In the absence of gravity, the flow along the vertical and horizontal center planes would be expected to be symmetric (donut-shaped), consistent with a purely thermocapillary-driven vortex at the meniscus. In the presence of gravity, however, symmetry is broken due to the combined action of surface tension and buoyancy forces. These forces are additive for the bottom vortex, making it stronger than the top vortex in which the surface tension and buoyancy forces oppose each other. The presence of the smaller top vortex visualized here is essential to realize a physically realizable 3D flow pattern. This is the first time that such a complete visualization of the combined buoyant-thermocapillary convection has been reported.

3.2 Buoyancy effect

The effect of gravity on the flow pattern was studied by observing the flow behavior along the vertical center plane for 200 and 75 μm diameter tubes.

< Figure 8 >

Long-exposure particle streak images along the vertical center plane are shown in Fig. 8(a, b). The small, closed arrows point to the location of the stagnation point on the meniscus. For the smallest diameter investigated (75 μm), a symmetric vortex pair is observed along the vertical center plane. This pattern displays asymmetry when the diameter is increased to 200 μm, although the extent of asymmetry is not as strong as for the 400 μm tube (Fig. 7). It is clear from these images that for the smaller length scales (~ 75 μm), gravity does not significantly influence the flow, whereas considerable buoyancy-driven asymmetry is induced at the larger length scales. The degree of asymmetry increases with tube size and a transition from steady axisymmetric

flow to steady asymmetric flow is observed to occur for a tube diameter between 75µm and 200 µm.

These effects due to buoyancy are also demonstrated through the numerical computations of Wang et al.[32]. These computed flow patterns near the meniscus for the symmetric and asymmetric cases exhibit qualitative agreement with the experimental results from the present work. To the authors' knowledge, this primary bifurcation of the flow pattern in such systems has not been experimentally observed to date.

4 Conclusions

Microfluidic visualization techniques were used to quantitatively explore the three-dimensional nature of thermocapillary convection pattern near an evaporating meniscus. µPIV measurements provided quantitative velocity measurements while long-exposure streak images illustrated the qualitative flow patterns. For small tube diameters (~ 75 µm), the effect of gravity on the flow pattern was found to be negligible and a single toroidal vortex was present near the meniscus. The flow pattern transition from an axisymmetric to an asymmetric toroidal pattern was visualized. The µPIV technique is shown to hold great promise for highly resolved flow field measurements near free surfaces. In ongoing work, tube size effects on thermocapillarity, buoyancy and evaporative flow rates over a wide range of tube diameters are being studied.

Acknowledgments

References

1. Schatz MF and Neitzel GP (2001) Experiments on thermocapillary instabilities. Ann Rev Fluid Mech 33:93-127
2. Scriven LE and Sternling CV (1960) Marangoni Effects. Nature. 187 (4733): 186-188
3. Buffone C, Sefiane K and Christy JRE (2005) Experimental investigation of self-induced thermocapillary convection for an evaporating meniscus in capillary tubes using micro-particle image velocimetry. Phys Fluids 17 (5): 052104
4. Davis SH (1987) Thermocapillary Instabilities. Ann Rev Fluid Mech 19 403-435
5. Behnia M, Stella F and Guj G (1995) A Numerical Study of 3-Dimensional Combined Buoyancy and Thermocapillary Convection. Int J Multiphase Flow. 21 (3): 529-542
6. Behnia M, Stella F and Guj G (1995) Numerical Study of 3-Dimensional Low-Pr Buoyancy and Thermocapillary Convection. Numerical Heat Transfer Part a-Applications. 27 (1): 73-88
7. Bergman TL and Ramadhyani S (1986) Combined Buoyancy-Driven and Thermocapillary-Driven Convection in Open Square Cavities. Numerical Heat Transfer. 9 (4): 441-451
8. Carpenter BM and Homsy GM (1989) Combined Buoyant Thermocapillary Flow in a Cavity. J Fluid Mech. 207: 121-132
9. Oron A, Davis SH and Bankoff SG (1997) Long-scale evolution of thin liquid films. Rev Modern Phys 69 (3): 931-980
10. Riley RJ and Neitzel GP (1998) Instability of thermocapillary-buoyancy convection in shallow layers. Part 1. Characterization of steady and oscillatory instabilities. J Fluid Mech. 359: 143-164
11. Smith MK and Davis SH (1983) Instabilities of Dynamic Thermocapillary Liquid Layers .1. Convective Instabilities. J Fluid Mech. 132: 119-144
12. Smith MK and Davis SH (1983) Instabilities of Dynamic Thermocapillary Liquid Layers .2. Surface-Wave Instabilities. J Fluid Mech. 132 : 145-162
13. Lee KJ, Kamotani Y and Yoda S (2002) Combined thermocapillary and natural convection in rectangular containers with localized heating. Int J Heat Mass Transfer. 45 (23): 4621-4630
14. Wozniak G, Wozniak K and Bergelt H (1996) On the influence of buoyancy on the surface tension driven flow around a bubble on a heated wall. Exp Fluids. 21 (3): 181-186
15. Wozniak K, Wozniak G and Roesgen T, (1989), Experimental investigation of the thermocapillary flow around a bubble by means of laser-speckle-velocimetry. In: Proceedings of the 7th European Symposium on Materials and Fluid Sciences in Microgravity
16. Wozniak K, Wozniak G and Roesgen T (1990) Particle-image-velocimetry applied to thermocapillary convection. Exp Fluids. 10 (1): 12-16
17. Kamotani Y, Ostrach S and Pline A (1994) Analysis of Velocity Data Taken in Surface-Tension Driven Convection Experiment in Microgravity. Phys Fluids 6 (11): 3601-3609
18. Braunsfurth MG and Homsy GM (1997) Combined thermocapillary-buoyancy convection in a cavity. Part II. An experimental study. Phys Fluids 9 (5): 1277
19. Ward CA and Duan F (2004) Turbulent transition of thermocapillary flow induced by water evaporation. Phys Rev E. 69 (5): 056308
20. Pratt DM and Hallinan KP (1997) Thermocapillary effects on the wetting characteristics of a heated curved meniscus. J Thermophys Heat Transfer. 11 (4): 519-525
21. Kim IY and Wayner PC (1996) Shape of an evaporating completely wetting extended meniscus. J Thermophys Heat Transfer. 10 (2): 320-325

22. Hohmann C and Stephan P (2002) Microscale temperature measurement at an evaporating liquid meniscus. Exp Thermal Fluid Sci 26 (2-4): 157-162

23. Swanson LW and Herdt GC (1992) Model of the Evaporating Meniscus in a Capillary-Tube. J Heat Transfer 114 (2): 434-441

24. Pratt DM, Brown JR and Hallinan KP (1998) Thermocapillary effects on the stability of a heated, curved meniscus. J Heat Transfer 120 (1): 220-226

25. Molenkamp T, (1998), Marangoni convection, mass transfer and microgravity. Universiteit Groningen.

26. Buffone C and Sefiane K (2004) Investigation of thermocapillary convective patterns and their role in the enhancement of evaporation from pores. Int J Multiphase Flow. 30 (9): 1071-1091

27. Buffone C, Sefiane K and Christy JRE (2004) Experimental investigation of the hydrodynamics and stability of an evaporating wetting film placed in a temperature gradient. Appl Thermal Engineering. 24 (8-9): 1157-1170

28. Buffone C, Sefiane K and Easson W (2005) Marangoni-driven instabilities of an evaporating liquid-vapor interface. Phys Rev E. 71 (5):

29. Santiago JG, Wereley ST, Meinhart CD, Beebe DJ and Adrian RJ (1998) A particle image velocimetry system for microfluidics. Exp Fluids. 25 (4): 316-319

30. Gui L and Wereley ST (2002) A correlation-based continuous window-shift technique to reduce the peak-locking effect in digital PIV image evaluation. Exp Fluids. 32 (4): 506-17

31. Meinhart CD, Wereley, S.T., and Santiago, J.G., (2000), Micron-Resolution Velocimetry Techniques, in Laser Techniques Applied to Fluid Mechanics, Adrian, R.J., Editor, Springer-Verlag: Berlin. p. 57-70.

32. Wang H, Garimella SV and Murthy JY, (2006), Transport from a volatile meniscus in a microtube.In: Proceedings 2006 ASME International Mechanical Engineering Congress and Exposition.Chicago, Illinois.

Ref 32 is now accepted for journal publication – it should indicate: International Journal of Heat and Mass Transfer (in press).

Table Captions

Table. 1. Velocity magnitudes along the horizontal center line of the seven planes of 400 µm tube at a distance approximately 80 µm away from the liquid-vapor interface.

Figure Captions

Fig. 1. Experimental setup for the horizontal cross-section μPIV measurements.

Fig. 2. (a) Raw image obtained in a FEP tube, in comparison to (b) a refractive-index-matched image obtained in a FEP tube.

Fig. 3. Modified experimental setup for vertical cross-section μPIV measurements.

Fig. 4. Cross section of the 400 μm diameter capillary tube showing the location of measurement planes.

Fig. 5. (a) Raw image of evaporating meniscus, and (b) plot of averaged error vs. number of image pairs.

Fig. 6. Velocity vectors with vorticity contours at different measurement planes identified in Fig. 4. (a) Top plane 3, (b) Top plane 2, (c) Top plane 1, (d) Horizontal center plane, (e) Bottom plane 1, (f) Bottom plane 2, (g) Bottom plane 3.

Fig. 7. Long-exposure particle streak image along the vertical center plane for the 400 μm tube. The locations of the seven measurement planes are also shown..

Fig. 8. Long-exposure particle streak images along the vertical center plane for tubes of diameter (a) 75 μm, and (b) 200 μm.

Table. 1

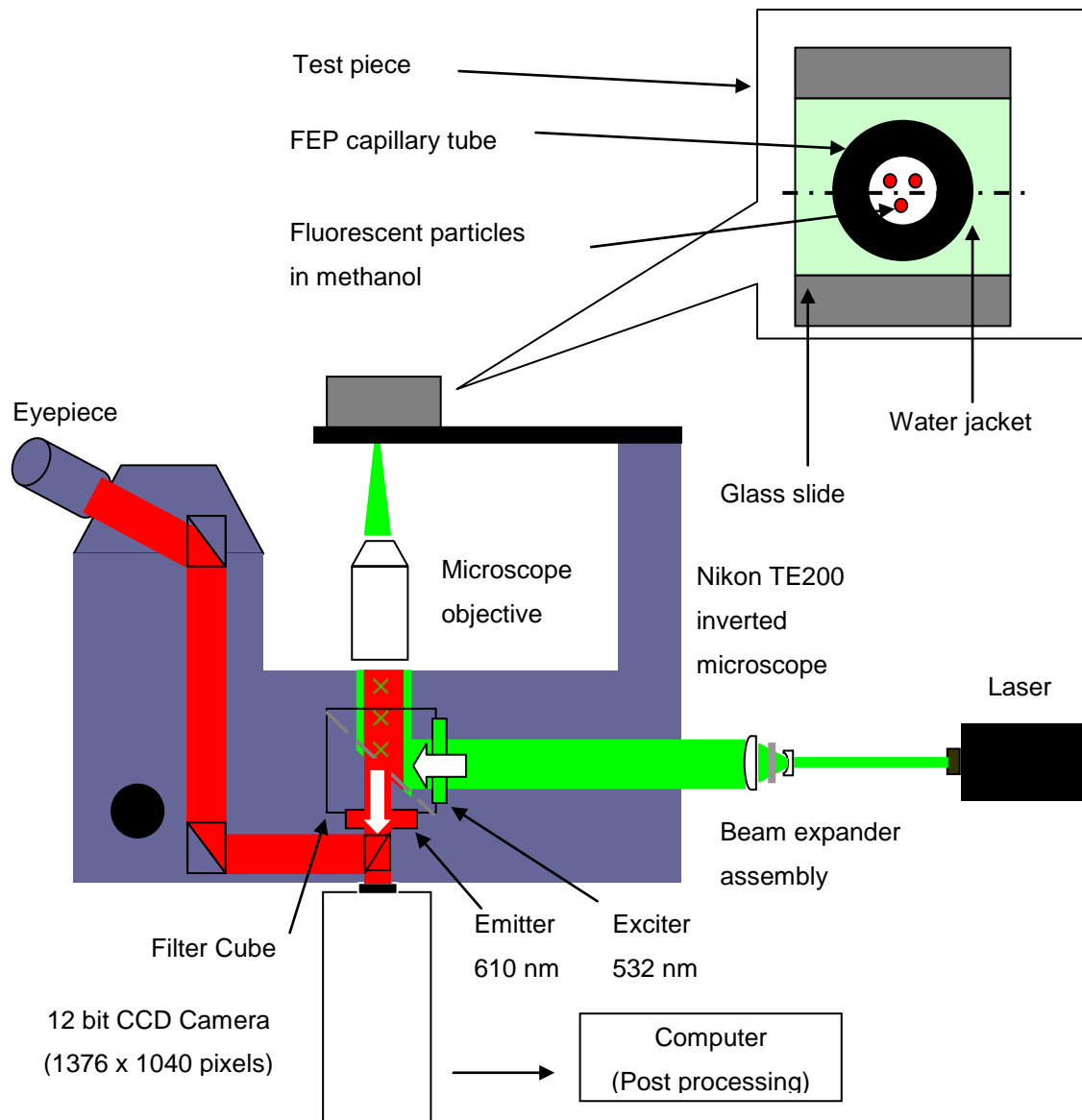| Plane	Velocity(μm/s)
Top plane 3 (+167 μm)	227
Top plane 2 (+133 μm)	434
Top plane 1 (+67 μm)	329
Horizontal center plane (0 μm)	107
Bottom plane 1 (-67 μm)	153
Bottom plane 2 (-133 μm)	303
Bottom plane 3 (-167 μm)	293

Fig. 1

Test piece

FEP capillary tube

Fluorescent particles
in methanol

Water jacket

Glass slide

Eyepiece

Microscope
objective

Nikon TE200
inverted
microscope

Laser

Beam expander
assembly

Emitter
610 nm

Exciter
532 nm

Filter Cube

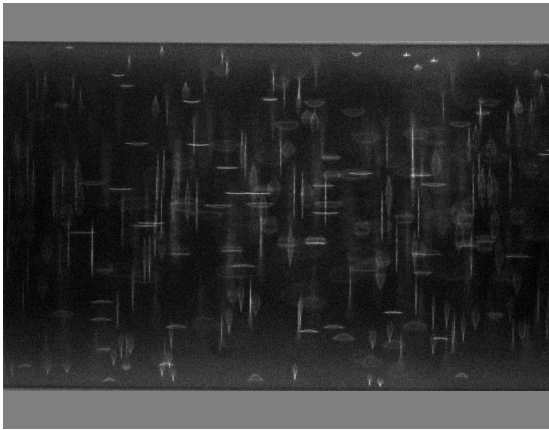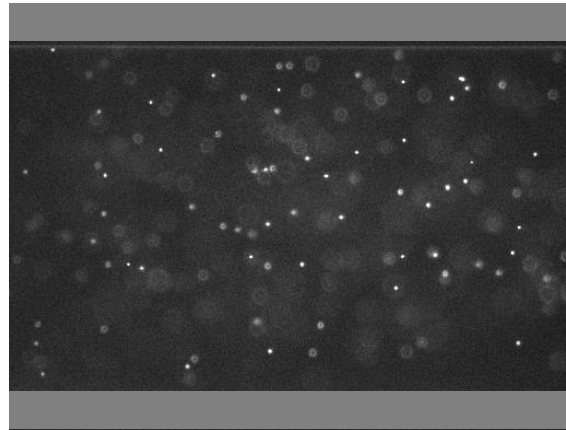12 bit CCD Camera
(1376 x 1040 pixels)

Computer
(Post processing)

Fig. 2

(a)   (b)

Fig. 3

Computer
(Post processing)

12 bit CCD Camera
(1376 x 1040 pixels)

Fluorescent particles in
methanol

FEP capillary
tube

Emitter
610 nm

Filter Cube

Microscope
Objective

Exciter
532 nm

Hg lamp

Glass slide

Water jacket

Test piece

Mirror

Nikon eclipse
microscope
ME600

Fig. 4

Top plane 3 (+167 μm)

Top plane 2 (+133 μm)

Top plane 1 (+67 μm)

Horizontal center plane (0 μm)

Bottom plane 1 (-67 μm)

Bottom plane 2 (-133 μm)

Bottom plane 3 (-167 μm)

Vertical center plane

Gravity

Fig. 5

(a)   (b)

Fig. 6

(a)

(b)

(c)

(d)

Tube Wall

Meniscus

Tube Wall

(g)

(f)

(e)

Fig. 7

Top plane 3 (+167 μm)

Top plane 2 (+133 μm)

Top plane 1 (+67 μm)

Horizontal center plane (0 μm)

Bottom plane 1 (-67 μm)

Bottom plane 2 (-133 μm)

Bottom plane 3 (-167 μm)

g

Fig. 8

(a)

(b)